Journal of Hazardous Materials 492 (2025) 138126

Contents lists available at ScienceDirect

Journal of Hazardous Materials

journal homepage: www.elsevier.com/locate/jhazmat

Health risks of ambient polycyclic aromatic hydrocarbons based on the prediction of their gas-phase concentrations in the central Yangtze River Delta, China: Regional and time-resolved variability

Wanqing Qi [a], Wei Feng [a], Xiangyu Zhang [a], Guihong Dong [a], Guofeng Shen [b], Zhijuan Shao [c], Ke Li [a], Hong Liao [a], Yuhang Wang [d], Mingjie Xie [a,*]

[a] Collaborative Innovation Center of Atmospheric Environment and Equipment Technology, Jiangsu Key Laboratory of Atmospheric Environment Monitoring and Pollution Control, School of Environmental Science and Engineering, Nanjing University of Information Science & Technology, 219 Ningliu Road, Nanjing 210044, China
[b] Laboratory for Earth Surface Processes, College of Urban and Environmental Sciences, Peking University, Beijing 100871, China
[c] School of Environment Science and Engineering, Suzhou University of Science and Technology Shihu Campus, 99 Xuefu Road, Suzhou 215009, China
[d] School of Earth and Atmospheric Sciences, Georgia Institute of Technology, Atlanta, GA 30332, United States

HIGHLIGHTS

- The benzo[*a*]pyrene equivalents of gas- and particle-phase PAHs were well reproduced.
- The health risks of total PAHs in the central YRD are homogeneously distributed.
- The daily cycle of total PAHs is shaped by various emission sources and meteorology.
- The contribution of gaseous PAHs to the total risk is over 40 % at midday in summer.

GRAPHICAL ABSTRACT

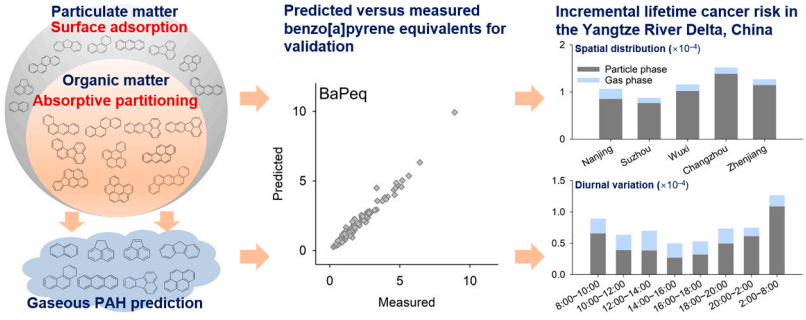

ARTICLE INFO

Key words:
Polycyclic aromatic hydrocarbon
Health effect
Gas-particle partitioning
Spatial variability
Diurnal profile

ABSTRACT

The health risks of ambient polycyclic aromatic hydrocarbons (PAHs) have widely been assessed using their particulate data, while PAHs in the gas phase have rarely been considered due to their lack of availability. In this study, an equilibrium model for gas-particle partitioning, including both absorption and adsorption mechanisms, was parameterized to predict PAHs in the gas phase from particle data. This model was validated using measured PAHs in the gas and particle phase (G + P) from northern Nanjing, China. It was found that the benzo[*a*]pyrene equivalents (BaPeq) of total G + P PAHs were well reproduced. After predicting gaseous PAHs for integrated $PM_{2.5}$ samples from five central cities in the Yangtze River Delta (YRD), China and time-resolved $PM_{2.5}$ samples from northern Nanjing, BaPeq of G + P PAHs showed high regional homogeneity in fall and winter, and gaseous PAHs contributed 43.6 % of the BaPeq and incremental lifetime cancer risk (ILCR) of G + P PAHs at noon in summer when the temperature was the highest. The regional variability and diurnal patterns of ambient PAHs

* Correspondence to: 219 Ningliu Road, Nanjing, Jiangsu 210044, China.
E-mail addresses: mingjie.xie@nuist.edu.cn, mingjie.xie@colorado.edu (M. Xie).

https://doi.org/10.1016/j.jhazmat.2025.138126
Received 2 February 2025; Received in revised form 30 March 2025; Accepted 31 March 2025
Available online 31 March 2025

and associated health risks presented in this study are important for an accurate assessment of personal inhalation exposure in the YRD region.

1. Introduction

Polycyclic aromatic hydrocarbons (PAHs) are a group of semi-volatile organic compounds (SVOCs) that originate from incomplete combustion processes and are ubiquitous in air, soil, and water. As many PAHs are known carcinogens (e.g., benzo[*a*]pyrene) and inhalation is an important exposure pathway for humans [42,58,6,71], the concentrations, spatiotemporal variability, and sources of PAHs in the atmosphere and their health effects have been intensively investigated [15,26,54,65]. In Western Europe and the United States, total PAH concentrations and associated health risks, typically expressed in benzo[*a*]pyrene (BaP) equivalents (BaPeq) and incremental lifetime cancer risk (ILCR), have been declining for decades due to stringent control measures for emission sources [29,33]. Specific standards or targets have been set up to minimize inhalation exposure to airborne PAHs. For example, the US Occupational Safety and Health Administration has established a permissible exposure level of 0.2 mg m^{-3} (8-hour time-weighted average) for PAHs in workplace air [3]. The European Union targets to limit the annual mean concentration of B[*a*]P in particulate matter (PM) with an aerodynamic diameter of less than 10 μm (PM_{10}) to no more than 1 ng m^{-3} [16], and the UK National Air Quality Objective for B[*a*]P in ambient air is even stricter with an annual mean value of 0.25 ng m^{-3} [13]. In 2020, only 7 of the 33 sampling sites in the UK PAH network exceeded 0.25 ng m^{-3} (0.27 – 0.84 ng m^{-3}; [9]).

According to Yan et al. [65] and the references therein, particulate PAHs in Chinese cities mainly originate from coal and biomass burning, motor vehicle emissions, and the coke and petroleum industries; PAH pollution was higher in northern cities than in southern cities due to large amounts of coal and biofuel used for heating in winter. Besides the changes in emission sources, the high winter and low summer levels of PAH pollution were also attributed to seasonal variations in meteorological conditions (e.g., temperature, precipitation, and solar radiation; [46,56]). Following the implementation of a series of air pollution control plans in China since 2013 ("Air Pollution Prevention and Control Action Plan", 2013–2017; the "Three-Year Blue Sky Action Plan", 2018–2020), PM pollution in Chinese cities decreased drastically [25,28,70]. The PAH emission inventory compiled by Wang et al. [55] showed an emission decrease of 11.4 % from 2013 to 2017 in mainland China. In Nanjing, a typical megacity in the Yangtze River Delta (YRD), China, the annual mean concentration of priority PAHs (excluding naphthalene) as defined by the US Environmental Protection Agency (EPA) in $PM_{2.5}$ decreased from 14.3 ng m^{-3} in 2014–2015 to 9.21 ng m^{-3} in 2018–2019 [20,24].

In most studies, the health risks of airborne PAHs were assessed only by measuring their concentrations in the particle phase [24,45,52,7], with integrated PM sampling performed at low temporal resolution (12–24 h). This may be because preparation for sampling gaseous PAHs and subsequent analysis is time- and solvent-consuming [20,63], and because continuous measurement technique for the gas-particle (G-P) partitioning of PAHs is not commercially available [32]. Ramírez et al. [43] reported BaPeq and ILCR of 18 parent PAHs in both gas and particle phase (G + P) near chemical industry sites in northeastern Spain for one year (2008–2009), and gas-phase PAHs accounted for 34–86 % of BaPeq and ILCR values for G + P PAHs. The spatial variability of PAH concentrations may jeopardize the representativeness of risk analysis based on measurement data at a single site. Some studies have performed multi-site sampling within a city to mitigate this issue [2,27,47,54]. However, the spatial distribution of PAHs and health risks at the regional level has scarcely been studied [15,26]. Since people spend time outdoors and indoors at different times of the day, time-resolved measurements of PAHs in air are beneficial not only for source identification and regulatory policy development, but also for accurate inhalation exposure estimation and risk analysis.

Central YRD is one of the most developed regions in China and suffers from air pollution problems [18,66]. To reveal the regional and diurnal variability of health risks of PAHs in this area, the integrated particle-phase concentrations ($PM_{2.5}$) of 15 parent PAHs in the five cities of southern Jiangsu (Nanjing, Suzhou, Wuxi, Changzhou, and Zhenjiang) from September, 2020 to February, 2021 were obtained from Feng et al. [18]. Time-resolved data of the same PAH species in $PM_{2.5}$ in northern Nanjing during the winter and summer of 2019 and 2020 were retrieved from Feng et al. [17]. The gas-phase concentrations of PAHs were predicted based on the above particle-phase data using an equilibrium partitioning model that accounts for both absorption and adsorption mechanisms [40,41], which was validated by using measured gas- and particle-phase data from northern Nanjing. The total concentrations of measured particle-phase and predicted gaseous PAHs were calculated to estimate the spatial and diurnal variations in their health risks. The results of the study will improve the understanding of the spatiotemporal variability of health risks from airborne PAHs in the central YRD and the estimation of personal inhalation exposure.

2. Methods

2.1. Data collection

The measurement results of 15 parent PAHs in $PM_{2.5}$ of the five central cities in the YRD were obtained from Feng et al. [18], where 23-h $PM_{2.5}$ samples were collected simultaneously every three days from September 1, 2020 to February 28, 2021 using a four-channel sampler with a flow rate of 16.7 L min^{-1}. The locations of the five sampling sites in Nanjing (Caochangmen), Suzhou (Nanmen), Wuxi (Environmental Monitoring Center), Changzhou (Environmental Monitoring Center), and Zhenjiang (Center for Disease Control and Prevention) are shown in Fig. 1. Time-resolved measurement data of PAHs in $PM_{2.5}$ from northern Nanjing were derived from Feng et al. [17], with 2-h $PM_{2.5}$ samples collected from 8:00–20:00 and 6-h samples collected from 20:00–8:00 (the next day) on each sampling day. The sampling site is located on the roof of a seven-story building of Nanjing University of Information Science and Technology (NUIST, Fig. 1). A total of 15-day sampling was conducted in winter 2019 (January, $N = 7$) and 2020 (January, $N = 8$), and 48-day sampling was conducted in summer 2019 (June–September, $N = 24$) and 2020 (June–September, $N = 24$). To test and validate the prediction method for PAH concentrations in the gas phase, the measurement results of PAH concentrations in $PM_{2.5}$ and in the gas phase from Gou et al. [20] were used. $PM_{2.5}$ and gas-phase samples were collected in pairs every sixth day (11–12 h sampling; twice daily) from September 2018 to September 2019 using a medium-volume sampler (300 L min^{-1}) at the same site (NUIST) in northern Nanjing (Fig. 1).

All six sampling sites are located in urban or suburban areas and are not close to point sources of emissions. The surrounding area consists mainly of residential buildings and road traffic. As shown in Fig. 1, the five cities in southern Jiangsu form the center of the YRD region, one of the most developed areas in China, and the selected sampling sites are almost evenly distributed. Feng et al. [18] reported a spatially homogeneous distribution of PAH concentrations and the main sources (industrial emissions and biomass burning) in the five cities of southern Jiangsu, indicating the dominance of regional emissions. In addition, the main factors influencing the G-P partitioning of PAHs, including $PM_{2.5}$ major components and meteorological parameters (temperature and relative humidity), also showed high spatial homogeneity in southern Jiangsu [18]. Therefore, the sampling sites selected in this study were

well representative of the central YRD region.

The analytical method for non-polar SVOCs, including PAHs, was described in detail in the studies mentioned above. Briefly, an aliquot of each $PM_{2.5}$-loaded quartz filter was pre-spiked with 20 μL of a mixture of isotopically labeled PAHs (internal standard, IS) and ultrasonically extracted twice with methylene chloride for 15 min. Gaseous SVOCs in adsorbent samples (polyurethane foam and XAD-4 resin cartridge) were pre-spiked with IS and Soxhlet-extracted in methylene chloride for 24 h. The extracts of the particulate and gaseous samples were filtered, concentrated, and examined using a gas chromatograph (GC, Agilent 7890B)-mass spectrometer (MS, Agilent 5977B). Six-point calibration curves were generated to determine the concentrations of each species following an internal standard method. Field blank corrections were performed before calculating the ambient concentrations of the target compounds. Moreover, the concentrations of bulk organic carbon (OC) and elemental carbon (EC) in filter samples were measured using a thermo-optical carbon analyzer (DRI Model 2001) according to the IMPROVE-A protocol. The $PM_{2.5}$ mass accumulated in each filter sample from the NUIST site was determined gravimetrically, and the synchronized $PM_{2.5}$ data of the five central YRD cities were obtained from the online air quality platform [53]. Table S1 in the Supporting Information lists the mean concentrations of 19 PAHs in $PM_{2.5}$ and gas phase, OC, and $PM_{2.5}$ mass at the NUIST site from 2018 to 2019. Chrysene and triphenylene have similar vapor pressure ($\sim 10^{-9}$ atm at 298.15 K; [21, 22]), and these two compounds cannot be separated on the stationary phase of the GC column (HP-5ms, Agilent) chosen for the analysis [20, 63]. Therefore, these two compounds were treated as one species (CHY/TP). For the same reason, benzo[*b*]fluoranthene and benzo[*k*]fluoranthene were grouped together as BbkF. Four PAHs with the lowest MW (naphthalene-NAP, acenaphthene-ACE, acenaphthylene-ACY, and fluorene-FLU) in $PM_{2.5}$ showed mean concentrations below the method detection limit (MDL, Table S1) and/or a high proportion of missing values. Their concentrations in $PM_{2.5}$ were not reported for the five central YRD cities [18] and the time-resolved samples at NUIST in northern Nanjing [17]. Therefore, the mean concentrations of 15 PAHs in $PM_{2.5}$, OC, and $PM_{2.5}$ mass from Nanjing, Suzhou, Wuxi, Changzhou, and Zhenjiang are summarized in Table S2; the mean concentrations during individual sampling intervals for time-resolved measurements are listed in Table S3.

2.2. Gas-phase PAH predictions and validation

The G-P partitioning of SVOCs was defined in early studies on the basis of the measured concentrations of the individual species in the particle and gas phase and the PM mass [39,64]:

$$K_p = \frac{F/\mathrm{TSP}}{A} \tag{1}$$

where K_p (m^3 μg^{-1}) is the partitioning coefficient, TSP (μg m^{-3}) is the concentration of total suspended particles (TSP), and F and A (ng m^{-3}) are the concentrations of each compound in the particle and gas phase, respectively. In this work, TSP was replaced by $PM_{2.5}$ mass in Eq. (1). Cui et al. [11] have shown that the particle-phase PAHs are enriched in $PM_{2.5}$ in northern Nanjing.

The partitioning coefficient can also be predicted using an equilibrium model developed by [40,41]:

$$K_p = \frac{1}{p_L^o}\left[N_s a_{TSP} RT e^{(Q_l - Q_v))/RT} + \frac{f_{OM} RT}{10^6 \mathrm{MW}_{OM} \zeta_{OM}}\right] \tag{2}$$

where p_L^o is the subcooled liquid vapor pressure (atm) of each PAH, and the first and second terms in the brackets represent the adsorption on PM surfaces and the absorptive partitioning to particulate organic matter (OM), respectively. In the first term, N_s (mol cm^{-2}) is the surface concentration of the adsorption sites, a_{TSP} (m^2 g^{-1}) denotes the specific surface area of TSP, and Q_l–Q_v (kJ mol^{-1}) is the difference between subcooled liquid desorption enthalpy (Q_l) and vaporization enthalpy (Q_v). To best fit the measured lg K_p of PAHs in northern Nanjing (China) and Denver (United States), Zhou et al. [72] developed a parameterization method for Eq. (2) by setting N_s and $a_{PM2.5}$ to 6.64×10^{-10} mol cm^{-2} and 10 m^2 g^{-1}, respectively. The Q_l–Q_v value for Denver (3 kcal mol^{-1}) was higher than that for Nanjing (2 kcal mol^{-1}), possibly due to the extremely low aerosol water content in Denver. Since the influencing factors for the G-P partitioning of PAHs and their sources in southern Jiangsu showed high spatial homogeneity (Section 2.1), the equilibrium model parameterized for describing G-P partitioning of

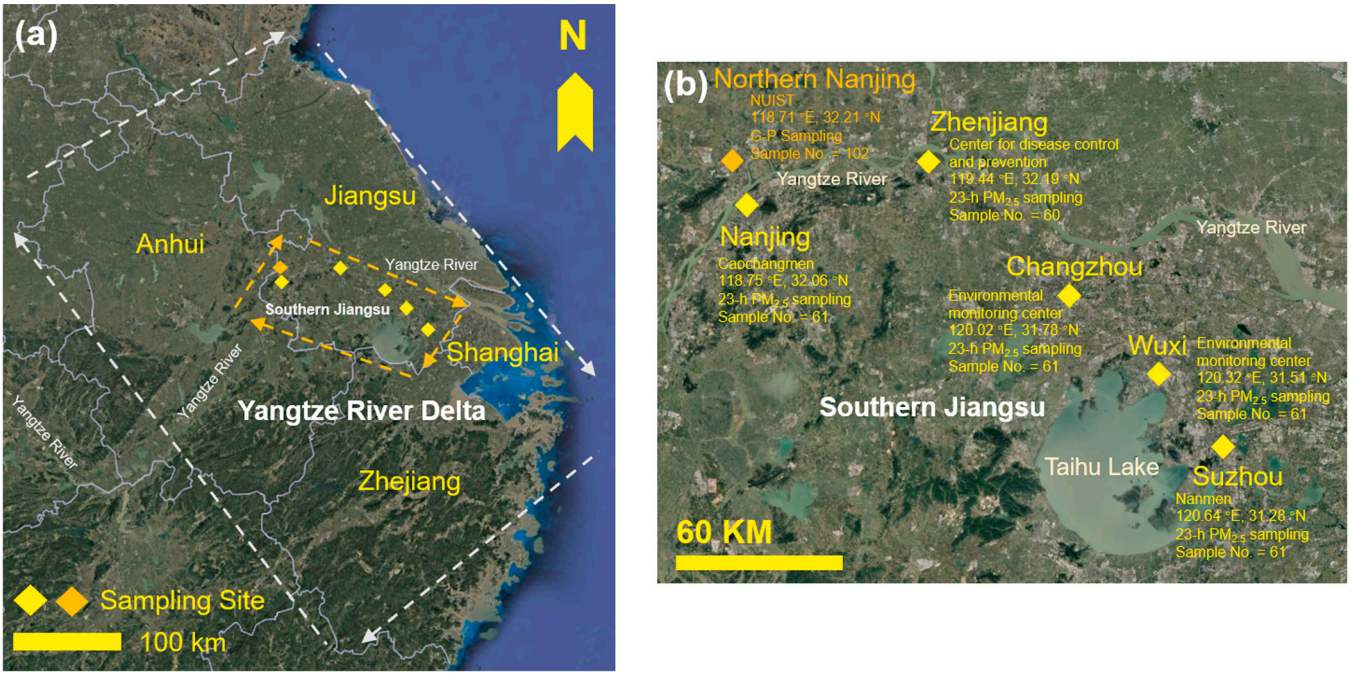

Fig. 1. Locations of sampling sites in (a) the Yangtze River Delta (YRD), eastern China, and (b) southern Jiangsu, center of the YRD region. Map data: Google earth [19].

PAHs in northern Nanjing by Zhou et al. [72] was used in this work. In the absorptive partitioning term, f_{OM} is the fraction of PM accounted for by OM, of which the concentration was calculated as OC× 1.6 [48]. MW_{OM} (g mol^{-1}) and ζ_{OM} are the mean molecular weight (MW) of particulate OM and the molar activity coefficient of a specific compound in particulate OM, respectively. To be consistent with previous studies, these two parameters were set to 200 g mol^{-1} and 1.0, respectively [20,4,61–63,72].

In both terms, R and T are the gas constant (8.21 ×10^{-5} m^3 atm mol^{-1} K^{-1}) and the ambient temperature (K). The p_L^o value of each PAH was calculated for each sample as follows

$$p_L^o = p_L^{o,*}\exp\left[\frac{Q_v^*}{R}\left(\frac{1}{298.15}-\frac{1}{T}\right)\right] \quad (3)$$

where $p_L^{o,*}$ and Q^*_v are p_L^o and Q_v at 298.15 K. In this study, the $p_L^{o,*}$ and Q^*_v values of the target PAHs were taken from the literature based on the dependence of GC retention times on temperature (Table 1; [21,22,37]). Since the ranges of $p_L^{o,*}$ and Q^*_v values in the literature were within an order of magnitude, their midranges were used for p_L^o calculation (Table 1). Subsequently, the gas-phase concentrations of PAHs for the five central YRD cities and time-resolved samples in northern Nanjing can be predicted by combining Eqs. (1) and (2).

To validate the prediction method, the PAH concentrations in the gas phase and the corresponding BaPeq for the integrated sampling at the NUIST site were initially predicted using measurement data from the particle phase, and then the measured and predicted concentrations and BaPeq in the gas-phase and G + P PAHs were compared. If absorptive partitioning was the dominant mechanism, the measured and predicted absorptive partitioning coefficient ($K_{p,OM}$, m^3 μg^{-1}) can be parameterized as

$$K_{p,OM} = \frac{K_p}{f_{OM}} = \frac{F/M_{OM}}{A} \quad (4)$$

$$K_{p,OM} = \frac{RT}{10^6 MW_{OM}\zeta_{OM}p^o{}_L} \quad (5)$$

Since the equilibrium absorptive partitioning has been widely used to describe the G-P partitioning of ambient SVOCs and to predict the formation of secondary organic aerosols (SOA) in laboratory and field studies [31,38,5,62,63,69], the prediction results by combining Eqs. (4) and (5) were also presented for comparison.

2.3. Risk assessment

In this study, the BaPeq of the target PAHs in each sample were calculated by multiplying the concentrations of each PAH by the corresponding toxic equivalency factors (TEFs) used to rank the carcinogenicity of PAHs with respect to BaP [12]. The TEFs of our target PAHs were proposed by Nisbet and LaGoy [36] and Larsen and Larsen [30] and are listed in Table 1. The measured concentrations of low MW PAHs (e.g., NAP and FLU) in the particle phase and high MW PAHs (e.g, BbkF and DahA) in the gas phase were mostly below the MDL. As suggested by Ramírez et al. [43] and US EPA [50], these measurements were replaced by half of the MDL in the calculation of BaPeq. The ILCR values of the individual PAHs were calculated as

$$ILCR = BaPeq \times UR \quad (6)$$

where UR is the unit risk of the ILCR of PAHs in the ambient. Based on the estimation of WHO [59,60], the value of UR in this study was set at 8.7 × 10^{-5} per ng m^{-3}, which corresponds to 8.7 cases per 100,000 people with chronic inhalation exposure to BaP at 1 ng m^{-3}.

3. Results and discussion

3.1. Validation for the prediction of gaseous PAHs

Table S4 compares the mean values of measured and predicted concentrations and BaPeq for gaseous and G + P PAHs in northern Nanjing. Because G + P NAP, ACE, ACY, and FLU account for only a very small proportion (mean 5.11 % ± 2.86 %) of the BaPeq of all target PAHs, and their low levels in $PM_{2.5}$ (Table S1) could lead to large uncertainties in the gas-phase prediction, the prediction results for these four species were not reported. According to the measured data, PHE, ANT, FLT, and PYR (MW ≤ 202) were mainly present in the gas phase, while other PAHs (MW ≥ 228) primarily existed in the particle phase; PHE and FLT dominated (61.7 % ± 8.35 %) the G + P concentrations of

Table 1
Vapor pressures (atm) and enthalpies of vaporization (kJ mol^{-1}) at 273.15 K of the target PAHs and their TEFs used in this study.

Compounds	Abbr.	$p_L^{o,*}$		Q^*_v		TEF
		Literature value	This study	Literature value	This study	
naphthalene	NAP	(3.68–4.22)× 10^{-4}[a]	3.95 × 10^{-4}	55.7–62[a]	58.8	0.001[e]
acenaphthene	ACE	(1.46–1.50)× 10^{-5}[a]	1.48 × 10^{-5}	70.5–71.4[a]	71.0	0.001[e]
acenaphthylene	ACY	2.07 × 10^{-5}[a]	2.07 × 10^{-5}	69.1[a]	69.1	0.001[e]
fluorene	FLU	(4.32–5.20)× 10^{-6}[a]	4.76 × 10^{-6}	74.4–75.1[a]	74.7	0.0005[f]
phenanthrene	PHE	(7.34–9.90)× 10^{-7}[a]	8.62 × 10^{-7}	79.0–81.4[a]	80.2	0.0005[f]
anthracene	ANT	(6.54–10.6)× 10^{-7}[a]	8.57 × 10^{-7}	79.1–81.7[a]	80.4	0.0005[f]
fluoranthene	FLT	(4.73–11.9)× 10^{-8}[a]	8.32 × 10^{-8}	86.8–90.2[a]	88.5	0.05[f]
pyrene	PYR	(3.76–8.62)× 10^{-8}[a]	6.19 × 10^{-8}	87.2–91.0[a]	89.1	0.001[f]
benz[*a*]anthracene	BaA	(1.84–3.76)× 10^{-9}[a]	2.80 × 10^{-9}	95.2–104[a]	99.8	0.005[f]
chrysene/triphenylene	CHY/TP	(1.68–1.76)× 10^{-9}[a]	1.72 × 10^{-9}	97.0–103[a]	100	0.03[f,g]
benzo[b&k]fluoranthene	BbkF	(7.51–12.8)× 10^{-11}[a]	1.02 × 10^{-10}	104–106[a]	105	0.1[e]
benzo[*j*]fluoranthene	BjF	(7.51–12.8)× 10^{-11}[b]	1.02 × 10^{-10}	104–106[b]	105	0.05[f]
benzo[*e*]pyrene	BeP	9.68 × 10^{-11}[a]	9.68 × 10^{-11}	105–108[a]	107	0.002[f]
benzo[*a*]pyrene	BaP	(5.83–9.24)× 10^{-11}[a]	7.54 × 10^{-11}	105–107[a]	106	1[f]
indeno[1,2,3-cd]pyrene	IDP	1.06 × 10^{-11}[c]	1.06 × 10^{-11}	109[c]	109	0.1[f]
benzo[ghi]perylene	BghiP	(4.24–4.27)× 10^{-12}[d]	4.26 × 10^{-12}	106[d]	106	0.02[f]
dibenz[ah]anthracene	DahA	(3.32–3.41)× 10^{-12}[d]	3.37 × 10^{-12}	106[d]	106	1.1[f]

[a] Haftka et al. [21] and references therein
[b] values of BbkF were used
[c] Odabasi et al. [37]
[d] Hanshaw et al. [22] and references therein
[e] Nisbet and LaGoy [36]
[f] Larsen and Larsen [30]
[g] the same TEF value was assumed for triphenylene as for chrysene.

all PAHs. As Table S4 shows, the mean concentrations of the predicted PHE, ANT, FLT, and PYR gas-phase concentrations are much closer to the measurements when using the absorption and adsorption mechanism (Abs + Ads) than when using the absorptive partitioning mechanism (Abs), which also explains the good agreement between the measured (31.0 ± 20.6 ng m^{-3}) and predicted G + P concentrations (39.5 ± 31.7 ng m^{-3}) of all PAHs. Although the Abs mechanism can well explain the G-P partitioning of *n*-alkanes in northern Nanjing, the measured $K_{p,OM}$ values of PAHs were several times higher than those predicted, indicating stronger sorption to the particle phase than absorption [72]. This could be due to the particular interactions (e.g., π-π conjugation) between PAHs and solid surfaces [10,73]. However, the gas-phase concentrations of PAHs with MW ≥ 228 were not well predicted, which had little effect on the predicted mean G + P concentrations of these species (Table S4). A possible explanation for this is that PAHs with high MW had trace levels in the gas phase (Table S1), whose signal intensity was probably influenced and overestimated by co-eluted compounds with similar ion fragments for GC-MS analysis. For the same reason, ANT concentrations in $PM_{2.5}$ were subject to large uncertainties, which could lead to the large difference between measured and predicted gas-phase and G + P concentrations (Table S4).

When calculating the BaPeq of individual PAHs, the total BaPeq of gas-phase and G + P PAHs also showed better agreement between measurements (0.48 ± 0.21 ng m^{-3}; 2.15 ± 1.51 ng m^{-3}) and predictions (0.28 ± 0.26 ng m^{-3}; 1.95 ± 1.53 ng m^{-3}) according to the Abs + Ads mechanism (Table S4). In Table 1, the TEF value of FLT (0.05) was 50–100 times higher than that of PHE, ANT, and PYR, the other three prominent PAHs in the gas phase, and its mean gas-phase concentration was no less than 20 % of the total (Table S4). Thus, FLT accounted for a large fraction (48.2 % ± 16.6 %) of the BaPeq of all PAHs in the gas phase for the measured data. As shown in Fig. 2a and b, the regression slope for the predicted versus measured concentrations of G + P PAHs is closer to unity (0.88) for the Abs + Ads mechanism than for the Abs mechanism (2.31). Although the Abs + Ads mechanism could not perfectly reproduce the variations in the concentrations of G + P PAHs, the scattering data for the predicted and measured BaPeq of G + P PAHs almost overlapped with the identity line (Fig. 2c). Given that the BaPeq of gas-phase PAHs averaged 28.9 % ± 14.9 % of the BaPeq of G + P PAHs in 2018–2019 and often exceeded 50 % in summer, the health risks of gas-phase PAHs in the central YRD should not be ignored and can be predicted when the measurement data are not available.

3.2. Regional variability of G+P PAHs and risks

Feng et al. [18] found that the particle-phase concentrations of PAHs in Nanjing, Suzhou, Wuxi, Changzhou, and Zhenjiang exhibited similar temporal variability (r = 0.78–0.97), with particulate PAHs peaking in December and January between September 1, 2020, and February 28, 2021. Considering the spatial homogeneity of PAHs in the particle phase, the significant increase in winter was attributed to the long-range transport of combustion aerosols from northern China and unfavorable meteorological conditions. In this study, the gas-phase concentrations of PAHs from the five central cities in the YRD region were predicted using the Abs + Ads mechanism. The mean concentrations and BaPeq of G + P PAHs in the five cities are shown in Table S5. Figs. S1 and 3 show time series of concentrations and health risks of G + P PAHs.

Unlike the temporal variations of particulate PAHs, the concentrations of G + P PAHs showed no obvious increases from fall to winter (Fig. S1). PHE, ANT, FLT, and PYR together contributed 85.3 % ± 10.7 %–91.5 % ± 7.29 % of all G + P PAHs in the five central cities of the YRD region from September to November 2020 (fall). With the decrease in temperature and increase in heating activities in northern China during winter, the mass fractions of other PAHs with higher MW (≥228) increased to 25.4 % ± 14.6 %–34.3 % ± 13.7 %. These results suggest that evaporation of unburned fossil fuels is likely an important source of light PAHs in warm seasons [23,57]. However, the BaPeq of G + P PAHs remained low in fall and high in winter and was mainly contributed by particulate PAHs (78.9 % ± 17.0 %–85.2 % ± 14.5 %). In Fig. 3, the PAH species with mean contributions to BaPeq greater than 5 % in the five cities are FLT (10.4 %–16.9 %), BbkF (5.66 %–6.07 %), BaP (49.8 %–53.5 %), IDP (5.48 %–5.84 %), and DahA (18.6 %–22.6 %), of which only FLT occurs mainly in the gas phase, with particle-phase fractions ranging from 18.4 % ± 17.2 to 24.4 % ± 20.3 %. Since FLT and BaP are the two main contributors to the BaPeq of G + P PAHs in September and early October, 2020 (Fig. 3), it was expected that the health risks of PAHs in the gas and particle phase would be comparable in summer.

The correlation coefficients (r) of G + P PAHs between two sampling sites in the five cities showed a wider range (0.14–0.73) than that of particle-phase PAHs (Fig. S2), indicating that the gas-phase PAHs were more influenced by local sources. This might be because long-range transport is subject to photochemical oxidations due to the faster processing rate in the gas phase [14,44]. Due to the dominance of particulate PAHs in the health risks in late fall and winter, the r values and coefficient of divergence (COD) of G + P BaPeq between sampling sites (r = 0.79 ± 0.04, COD = 0.25 ± 0.04) are comparable to particulate BaPeq (r = 0.74 ± 0.10, COD = 0.30 ± 0.05; Fig. S2). Thus, the concentrations of G + P PAHs determined in one of the five cities can be used to evaluate and illustrate the health risks in the central YRD region during the cold period.

As shown in Fig. 3f, the ILCR values of G + P PAHs in the five cities are in the range of $1 \times 10^{-5} \times 10^{-4}$ in fall and winter, and the mean values are all higher than 1×10^{-4} in winter ($1.16 \times 10^{-4} \pm 6.84 \times 10^{-5}$–$2.00 \times 10^{-4} \pm 1.11 \times 10^{-4}$). The ILCR values in the cold

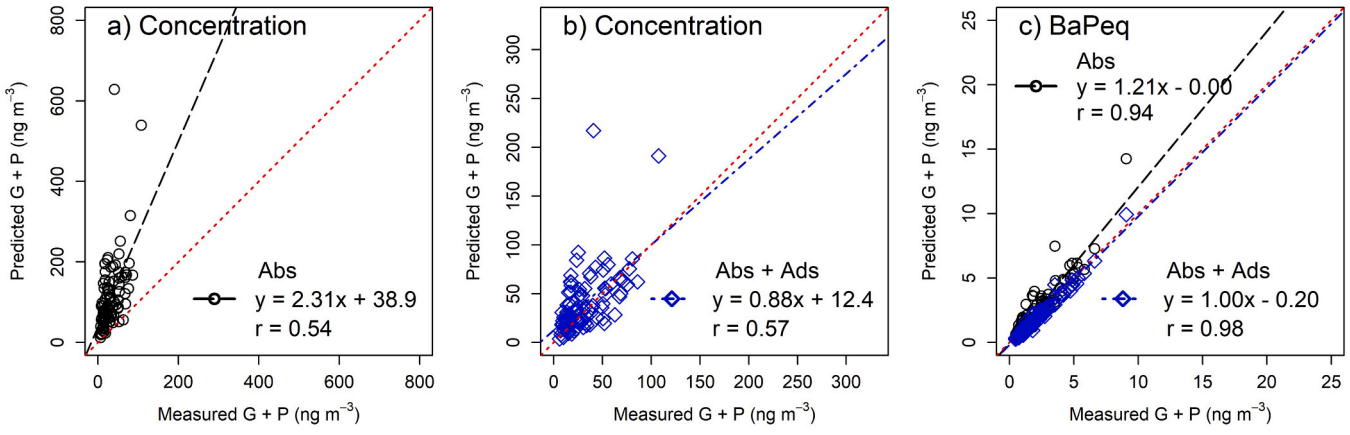

Fig. 2. Comparisons of measured and predicted (a, b) concentrations and (c) BaPeq of total G + P PAHs using Abs and Abs + Ads mechanisms.

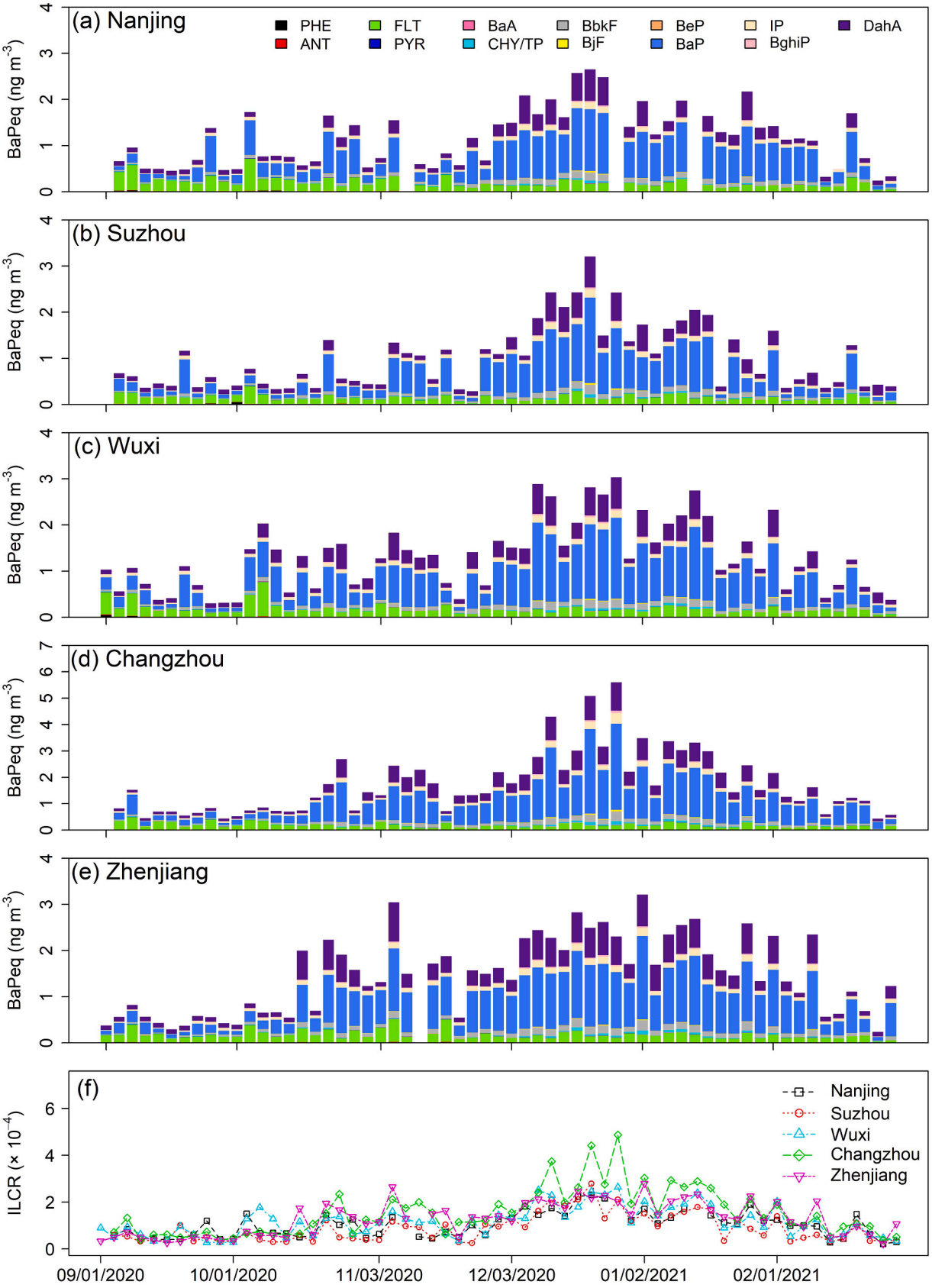

Fig. 3. Time series of stacked BaPeq (a-e) and total LLCR (f) of G + P PAHs in the five central cities of the Yangtze River Delta.

periods of this study were comparable to those of G + P PAHs at chemical industry sites in Spain (1.2×10^{-4}; [43]), but lower than those observed in two typical foundry plants in central Taiwan (9.06×10^{-4} and 1.09×10^{-3}; [34]). An ILCR value of 1×10^{-4} for PAHs was deemed unacceptable by the US EPA [49]. It was derived by setting a statewide standard of 1×10^{-5} for each carcinogen and assuming that no more than ten carcinogens would be detected at a site. Considering the spatial homogeneity of BaPeq (Figs. 3 and S2) and the high ILCR values ($> 1 \times 10^{-4}$) in winter in the central YRD region, joint prevention and control measures such as replacing coal and biomass fuels with cleaner energy (e.g., natural gas and electricity) should be continued to reduce PAH emissions during the heating season in northern China.

3.3. Time-resolved variability of G+P PAHs and risks

Feng et al. [17] reported a significant increase in $PM_{2.5}$ PAHs during the late afternoon rush hour only in winter for the northern Nanjing site, and the diurnal profile in summer was probably determined by the variations in planetary boundary layer height (PBLH). The increase in $PM_{2.5}$ PAHs at 16:00–20:00 in winter shown in Fig. S3a could also be partly related to the emissions from domestic heating (e.g., cooking) using biofuels in the neighboring rural areas [1,35]. The total concentrations of $PM_{2.5}$ PAHs reached their maxima at 8:00–10:00 am in winter (21.2 ng m^{-3}) and at 2:00–8:00 am in summer (6.53 ng m^{-3}; Table S3). Besides the influences of PBLH variations, particulate PAHs are more subject to photodegradation and evaporation at 8:00–10:00 am in summer than in winter, as sunrise occurs much earlier in summer (before 6:00 am). According to the measured particulate and predicted G + P PAHs, the mean particulate fraction of total PAHs was more than twice as high at 2:00–8:00 am (20.7 %) as at 8:00–10:00 am (9.20 %) in summer, while the values in the two sampling intervals in winter (62.2 % and 72.1 %) were comparable. Moreover, the earlier morning rush hour in summer (before 8:00 am) could also contribute to the highest $PM_{2.5}$ PAH concentrations at 2:00–8:00 am. In both winter and summer, PAH concentrations in the gas phase were much higher during the day than at night (Fig. S3b, e), and the particulate fractions of PAHs reached the lowest value at 14:00–16:00 (winter 46.3 %; summer 4.03 %) with the highest temperature. Although the mean difference between the daily maximum and minimum temperatures in winter and summer was only 4.72 ℃ and 6.82 ℃, respectively, the p_L^0 of individual PAHs increased by about 100 % from the lowest to the highest temperatures on both winter and summer days. In winter, total concentrations of particle-phase PAHs during individual sampling intervals (mean 10.5–21.2 ng m^{-3}) were generally higher than those of gas-phase PAHs (5.31–14.2 ng m^{-3}), and the diurnal profile of G + P PAHs was similar to that of the particle-phase PAHs (Fig. S3a, c). In contrast, G + P concentrations in summer were mainly determined by gas-phase PAHs (79.6 %–96.1 %) and showed a diurnal pattern identical to that of the gas phase (Fig. S3e, f).

Compared with gaseous pollutants and $PM_{2.5}$ major components in Nanjing [67,68], the diurnal patterns of $PM_{2.5}$, gaseous, and G + P PAHs in winter were similar to those of NO_2 and EC with elevated concentrations in the morning and late afternoon (Fig. S3a–c), indicating influences of commuting emissions. However, it cannot be ruled out that the biomass burning for heating purposes makes a contribution. In summer, the diurnal variations of gaseous and G + P PAHs (Fig. S3e, f) were similar to those of SO_2 and SO_4^{2-} with a broad peak during the day [17,68], reflecting the daily cycles of industrial emissions. Moreover, the higher temperature during the day could also contribute to the increased concentrations of G + P PAHs due to the evaporation of unburned fossil fuels. Photolysis and reactions with oxidants (e.g., ·OH and O_3) are important pathways for the degradation of PAHs in the atmosphere [51]. The intensity of solar radiation, which is reflected in temperature, reaches its maximum at around 12:00–16:00, and the highest O_3 concentrations in the YRD region occur at 14:00–16:00 [68,8], which could be a possible reason for the decrease in concentrations of gas-phase and G + P PAHs at 14:00–16:00.

Similar to the BaPeq composition in the five central YRD cities during fall and winter, only FLT, BbkF, BaP, IDP, and DahA contributed more than 5 % (daily weighted average 6.52 %–48.6 %) to the BaPeq of G + P PAHs of the time-resolved samples in winter (Fig. 4b). As the mean concentrations of FLT in the particle phase during each sampling interval (1.78–3.74 ng m^{-3}) were higher than the concentrations in the gas phase (0.89–2.21 ng m^{-3}) in winter, and particulate PAHs accounted for more than 90 % of the BaPeq of G + P PAHs, the inclusion of PAHs in the gas phase had little impact on the values or diurnal variations of total BaPeq and ILCR (Fig. 4a–c). In summer, FLT contributed 1.38 %–2.26 % and 13.5 %–39.7 % to the BaPeq of particulate and G + P PAHs, respectively, at different sampling intervals of the day; particulate PAHs accounted for 56.4 %–85.9 % of the BaPeq of G + P PAHs. In contrast to the diurnal pattern of G + P PAHs (Fig. S3e), the variations of G + P BaPeq and ILCR on summer days (Fig. 4e, f) were similar to those of PAHs in the particle phase (Fig. S3d). However, BaPeq or ILCR values of all PAHs could be underestimated by up to 43.6 % (12:00–14:00) when gas-phase PAHs were not considered, and the difference in BaPeq or ILCR between particulate and G + P PAHs reflected the diurnal pattern of FLT contributions.

In northern Nanjing, the mean ILCR value of total PAHs for different sampling intervals on winter days ranged from 1.19×10^{-4} to 2.57×10^{-4}, all of which were above the upper limit of the acceptable level (1×10^{-4}) set by the US EPA [49]. The ILCR value for winter days peaked at 18:00–20:00 (2.57×10^{-4}), largely due to increased traffic during rush hours and local biomass burning for domestic heating. The summertime ILCR exceeded 1×10^{-4} only at 2:00–8:00 am (1.26×10^{-4}), when the PBLH reached its daily minimum with the lowest temperature and the photodegradation of PAHs was weakest.

4. Conclusions and implications

Referring to the comparisons between measured and predicted G + P PAHs in northern Nanjing, the BaPeq of total G + P PAHs based on measured data can be reproduced by predicting the PAHs in the gas phase using an equilibrium G-P partitioning model that accounts for both absorption and adsorption mechanisms. Since the PAHs in the gas phase are mainly composed of low MW PAHs, the G + P PAHs in the central YRD region during fall and winter exhibited greater spatial heterogeneity than the particulate PAHs. However, the BaPeq values of both particulate and G + P PAHs were homogeneously distributed, suggesting that the measurement results of PAHs at a well-selected site can be used to assess their health effects in the central YRD region during the cold periods. The diurnal profile of G + P PAHs in winter reflected the influence of changes in PBLH, motor vehicle emissions during rush hours, and biomass burning for domestic heating, while the profile in summer was likely driven by industrial emissions and meteorology. Because the BaPeq of G + P PAHs in winter was predominantly determined by particulate PAHs, the inclusion of gas-phase PAHs had little impact on the value and diurnal profile of total BaPeq and ILCR. However, the time-resolved BaPeq values of particulate and G + P PAHs in summer showed significant ($p < 0.01$) differences that varied with temperature. In this work, the concentrations of G + P PAHs and their health effects were obtained at the end or immediately after the two nationwide air pollution control plans mentioned in the *Introduction*, and can be used as a reference for comparison in central YRD after the implementation of the subsequent air pollution control plans.

Environmental implications

Since the health risks associated with PAHs in the gas phase cannot be neglected during warm periods, the method used in this study can be used to predict PAH concentrations in the gas phase in a region with similar meteorological conditions and PM composition. Considering the spatial homogeneity of PAH health risks in the central Yangtze River

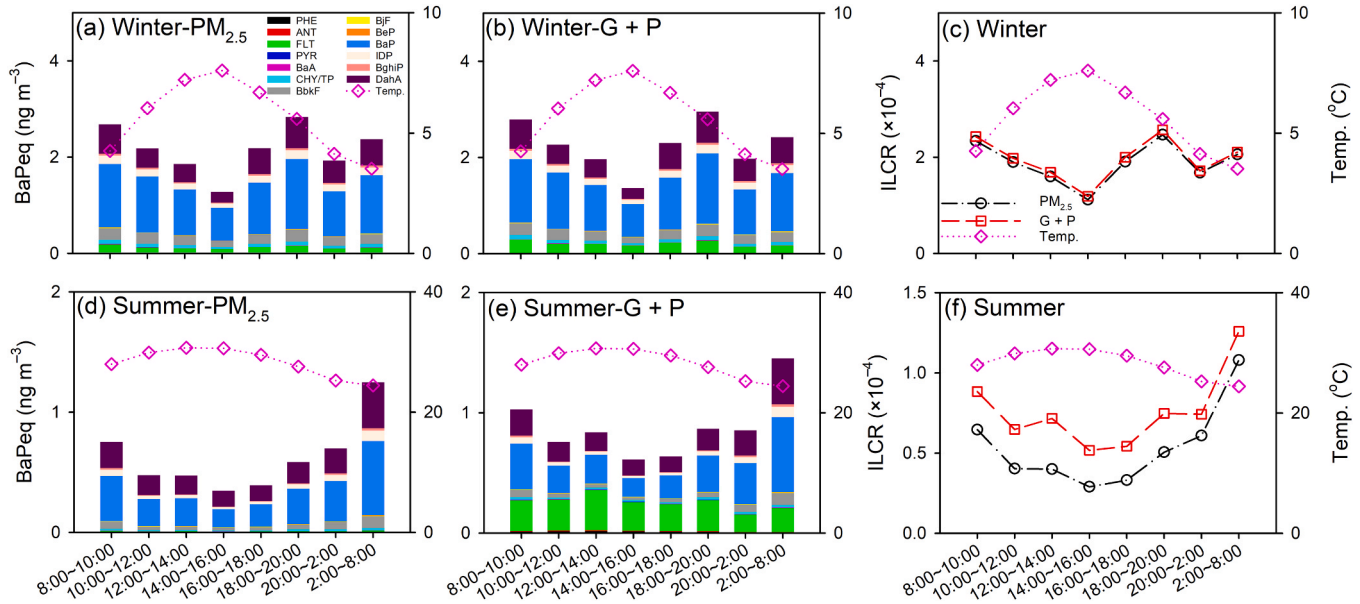

Fig. 4. Diurnal variations of stacked BaPeq of particulate (a, d) and G + P PAHs (b, e) and total LLCR of G + P PAHs (c, f) during winter and summer in northern Nanjing.

Delta (YRD), China, measurement-based assessment at a well-selected site may have good representativeness. The diurnal pattern of ambient PAHs and their health risks unveiled in this work can be used to achieve a better estimation of personal exposure risk in the YRD region.

CRediT authorship contribution statement

Qi Wanqing: Writing – original draft, Investigation, Data curation. **Feng Wei:** Investigation, Data curation. **Zhang Xiangyu:** Visualization, Investigation. **Dong Guihong:** Validation, Investigation. **Shen Guofeng:** Writing – review & editing. **Shao Zhijuan:** Writing – review & editing. **Li Ke:** Writing – review & editing, Resources, Funding acquisition. **Liao Hong:** Writing – review & editing, Resources. **Wang Yuhang:** Writing – review & editing, Resources. **Xie Mingjie:** Writing – review & editing, Supervision, Project administration, Methodology, Conceptualization.

Declaration of Competing Interest

The authors declare that they have no known competing financial interests or personal relationships that could have appeared to influence the work reported in this paper.

Acknowledgements

This work was supported by the National Key Research and Development Program of China (No. 2022YFE0136100) and the National Natural Science Foundation of China (NSFC, 42177211). We thank Yue Shang, Yafeng Gou, Li Yang, and Zhenzhen Zhao from Nanjing University of Information Science and Technology for their help with sampling and chemical analysis. We also thank Nanjing Environmental Monitoring Center of Jiangsu Province for assistance in sampling.

Appendix A. Supporting information

Supplementary data associated with this article can be found in the online version at doi:10.1016/j.jhazmat.2025.138126.

Data availability

Data will be made available on request.

References

[1] Alam, M.S., Keyte, I.J., Yin, J., Stark, C., Jones, A.M., Harrison, R.M., 2015. Diurnal variability of polycyclic aromatic compound (PAC) concentrations: relationship with meteorological conditions and inferred sources. Atmos Environ 122, 427–438. https://doi.org/10.1016/j.atmosenv.2015.09.050.

[2] Anastasopoulos, A.T., Wheeler, A.J., Karman, D., Kulka, R.H., 2012. Intraurban concentrations, spatial variability and correlation of ambient polycyclic aromatic hydrocarbons (PAH) and PM2.5. Atmos Environ 59, 272–283. https://doi.org/10.1016/j.atmosenv.2012.05.004.

[3] ATSDR, 1995. US: Agency for Toxic Substances and Disease Registry, Toxicological profile for polycyclic aromatic hydrocarbons (PAHs). U.S. Department of Health and Human Services, Public Health Service, Atlanta, GA.

[4] Barsanti, K.C., Pankow, J.F., 2004. Thermodynamics of the formation of atmospheric organic particulate matter by accretion reactions—Part 1: aldehydes and ketones. Atmos Environ 38, 4371–4382. https://doi.org/10.1016/j.atmosenv.2004.03.035.

[5] Beardsley, R.L., Jang, M., 2016. Simulating the SOA formation of isoprene from partitioning and aerosol phase reactions in the presence of inorganics. Atmos Chem Phys 16, 5993–6009. https://doi.org/10.5194/acp-16-5993-2016.

[6] Boström, C.-E., Gerde, P., Hanberg, A., Jernström, B., Johansson, C., Kyrklund, T., et al., 2002. Cancer risk assessment, indicators, and guidelines for polycyclic aromatic hydrocarbons in the ambient air. Environ Health Perspect 110, 451–488. https://doi.org/10.1289/ehp.110-1241197.

[7] Chen, X.-C., Ward, T.J., Ho, K.-F., Sarkar, C., Webster, C., 2022. Characteristics and health risks of personal exposure to particle-bound PAHs for Hong Kong adult residents: from ambient pollution to indoor exposure. Indoor Air 32, e12956. https://doi.org/10.1111/ina.12956.

[8] Chen, Z., Liu, R., Wu, S., Xu, J., Wu, Y., Qi, S., 2024. Diurnal variation characteristics and meteorological causes of autumn ozone in the Pearl River Delta, China. Sci Total Environ 908, 168469. https://doi.org/10.1016/j.scitotenv.2023.168469.

[9] Conolly, C., and Wu, H.: UK PAH Monitoring and Analysis Network 2020, Report for the Environment Agency Customer. Ref: ED12330AR2020- Issue Number 1, Ricardo Energy & Environment, United Kingdom, 2021.

[10] Cousins, I.T., Mackay, D., 2001. Gas–particle partitioning of organic compounds and its interpretation using relative solubilities. Environ Sci Technol 35, 643–647. https://doi.org/10.1021/es001123m.

[11] Cui, W., Wang, Z., Feng, W., Qin, C., Liao, H., Wang, Y., et al., 2025. Evaluating coarse PM composition and sources based on bulk and molecular speciation of PM2.5 and PM10 in Nanjing, East China. J Environ Sci 152, 155–166. https://doi.org/10.1016/j.jes.2024.04.038.

[12] Delistraty, D., 1997. Toxic equivalency factor approach for risk assessment of polycyclic aromatic hydrocarbons. Toxicol Environ Chem 64, 81–108. https://doi.org/10.1080/02772249709358542.

[13] Defra: Department for Environment, Food and Rural Affairs, The Air Quality Strategy for England, Scotland, Wales and Northern Ireland (volumes 1 and 2). London, UK, 2007.
[14] Donahue, N.M., Chuang, W., Epstein, S.A., Kroll, J.H., Worsnop, D.R., Robinson, A. L., et al., 2013. Why do organic aerosols exist? Understanding aerosol lifetimes using the two-dimensional volatility basis set. Environ Chem 10, 151–157. https://doi.org/10.1071/EN13022.
[15] Eiguren-Fernandez, A., Miguel, A.H., Froines, J.R., Thurairatnam, S., Avol, E.L., 2004. Seasonal and spatial variation of polycyclic aromatic hydrocarbons in vapor-phase and PM2.5 in Southern California urban and rural communities. Aerosol Sci Technol 38, 447–455. https://doi.org/10.1080/02786820490449511.
[16] European Union: Directive 2004/107/EC of the European Parliament and of the Council of 15 December 2004 Relating to Arsenic, Cadmium, Mercury, Nickel and Polycyclic Aromatic Hydrocarbons in Ambient Air. Official Journal of the European Union, 26 January 2005, L 23/3.
[17] Feng, W., Wang, X., Shao, Z., Liao, H., Wang, Y., Xie, M., 2023. Time-resolved measurements of PM2.5 chemical composition and brown carbon absorption in Nanjing, East China: diurnal variations and organic tracer-based PMF analysis. J Geophys Res Atmos 128, e2023JD039092. https://doi.org/10.1029/2023JD039092.
[18] Feng, W., Dong, G., Qi, W., Wang, Y., Zhang, X., Li, K., et al., 2024. Spatiotemporal variations of PM2.5 organic molecular markers in five central cities of the Yangtze River Delta, East China in autumn and winter: implications for regional and local sources of organic aerosols. Environ Pollut 363, 125227. https://doi.org/10.1016/j.envpol.2024.125227.
[19] Google earth V7.3.6.9796. (Imagery data: January 1, 2024). Terrametrics 2024. ⟨https://earth.google.com/web/⟩ (Last accessed, 25 November 2024).
[20] Gou, Y., Qin, C., Liao, H., Xie, M., 2021. Measurements, gas/particle partitioning, and sources of nonpolar organic molecular markers at a suburban site in the west Yangtze River Delta, China. J Geophys Res Atmos 126, e2020JD034080. https://doi.org/10.1029/2020JD034080.
[21] Haftka, J.J.H., Parsons, J.R., Govers, H.A.J., 2006. Supercooled liquid vapour pressures and related thermodynamic properties of polycyclic aromatic hydrocarbons determined by gas chromatography. J Chromatogr A 1135, 91–100. https://doi.org/10.1016/j.chroma.2006.09.050.
[22] Hanshaw, W., Nutt, M., Chickos, J.S., 2008. Hypothetical thermodynamic properties. subcooled vaporization enthalpies and vapor pressures of polyaromatic hydrocarbons. J Chem Eng Data 53, 1903–1913. https://doi.org/10.1021/je800300x.
[23] Hawthorne, S.B., Grabanski, C.B., 2000. Vaporization of polycyclic aromatic hydrocarbons (PAHs) from sediments at ambient conditions. Environ Sci Technol 34, 4348–4353. https://doi.org/10.1021/es001199i.
[24] Hong, Y., Xu, X., Liao, D., Ji, X., Hong, Z., Chen, Y., et al., 2021. Air pollution increases human health risks of PM2.5-bound PAHs and nitro-PAHs in the Yangtze River Delta, China. Sci Total Environ 770, 145402. https://doi.org/10.1016/j.scitotenv.2021.145402.
[25] Huang, J., Pan, X., Guo, X., Li, G., 2018. Health impact of China's air pollution prevention and control action plan: an analysis of national air quality monitoring and mortality data. Lancet Planet Health 2, e313–e323. https://doi.org/10.1016/S2542-5196(18)30141-4.
[26] Jedynska, A., Hoek, G., Eeftens, M., Cyrys, J., Keuken, M., Ampe, C., et al., 2014. Spatial variations of PAH, hopanes/steranes and EC/OC concentrations within and between European study areas. Atmos Environ 87, 239–248. https://doi.org/10.1016/j.atmosenv.2014.01.026.
[27] Jia, C., Fu, X., Jiang, Y., Nored, A., Smith, L., 2023. Spatiotemporal variability and measurement uncertainty in atmospheric polycyclic aromatic hydrocarbons (PAHs): a quantitative variance component analysis. Atmos Environ 302, 119735. https://doi.org/10.1016/j.atmosenv.2023.119735.
[28] Kan, H., 2022. World Health Organization air quality guidelines 2021: implication for air pollution control and climate goal in China. Chin Med J 135, 513–515. https://doi.org/10.1097/CM9.0000000000002014.
[29] Kim, K.-H., Jahan, S.A., Kabir, E., Brown, R.J.C., 2013. A review of airborne polycyclic aromatic hydrocarbons (PAHs) and their human health effects. Environ Int 60, 71–80. https://doi.org/10.1016/j.envint.2013.07.019.
[30] Larsen, J., Larsen, P., 1998. In: Hester, R.E., Harrison, R.M. (Eds.), Chemical Carcinogens in Air Pollution and Health. The Royal Society of Chemistry, Cambridge, UK.
[31] Liang, C., Pankow, J.F., Odum, J.R., Seinfeld, J.H., 1997. Gas/particle partitioning of semivolatile organic compounds to model inorganic, organic, and ambient smog aerosols. Environ Sci Technol 31, 3086–3092. https://doi.org/10.1021/es9702529.
[32] Liang, Y., Wernis, R.A., Kristensen, K., Kreisberg, N.M., Croteau, P.L., Herndon, S. C., et al., 2023. Gas–particle partitioning of semivolatile organic compounds when wildfire smoke comes to town. Atmos Chem Phys 23, 12441–12454. https://doi.org/10.5194/acp-23-12441-2023.
[33] Liu, B., Xue, Z., Zhu, X., Jia, C., 2017. Long-term trends (1990–2014), health risks, and sources of atmospheric polycyclic aromatic hydrocarbons (PAHs) in the U.S. Environ Pollut 220, 1171–1179. https://doi.org/10.1016/j.envpol.2016.11.018.
[34] Liu, H.-H., Yang, H.-H., Chou, C.-D., Lin, M.-H., Chen, H.-L., 2010. Risk assessment of gaseous/particulate phase PAH exposure in foundry industry. J Hazard Mater 181, 105–111. https://doi.org/10.1016/j.jhazmat.2010.04.097.
[35] Morville, S., Delhomme, O., Millet, M., 2011. Seasonal and diurnal variations of atmospheric PAH concentrations between rural, suburban and urban areas. Atmos Pollut Res 2, 366–373. https://doi.org/10.5094/APR.2011.041.
[36] Nisbet, I.C.T., LaGoy, P.K., 1992. Toxic equivalency factors (TEFs) for polycyclic aromatic hydrocarbons (PAHs). Regul Toxicol Pharmacol 16, 290–300. https://doi.org/10.1016/0273-2300(92)90009-X.
[37] Odabasi, M., Cetin, E., Sofuoglu, A., 2006. Determination of octanol–air partition coefficients and supercooled liquid vapor pressures of PAHs as a function of temperature: application to gas–particle partitioning in an urban atmosphere. Atmos Environ 40, 6615–6625. https://doi.org/10.1016/j.atmosenv.2006.05.051.
[38] Odum, J.R., Hoffmann, T., Bowman, F., Collins, D., Flagan, R.C., Seinfeld, J.H., 1996. Gas/particle partitioning and secondary organic aerosol yields. Environ Sci Technol 30, 2580–2585. https://doi.org/10.1021/es950943+.
[39] Pankow, J.F., Bidleman, T.F., 1992. Interdependence of the slopes and intercepts from log-log correlations of measured gas-particle partitioning and vapor pressure—I. theory and analysis of available data. Atmos Environ Part A Gen Top 26, 1071–1080. https://doi.org/10.1016/0960-1686(92)90039-n.
[40] Pankow, J.F., 1994. An absorption model of gas/particle partitioning of organic compounds in the atmosphere. Atmos Environ 28, 185–188. https://doi.org/10.1016/1352-2310(94)90093-0.
[41] Pankow, J.F., 1994. An absorption model of the gas/aerosol partitioning involved in the formation of secondary organic aerosol. Atmos Environ 28, 189–193. https://doi.org/10.1016/1352-2310(94)90094-9.
[42] Pashin, Y.V., Bakhitova, L.M., 1979. Mutagenic and carcinogenic properties of polycyclic aromatic hydrocarbons. Environ Health Perspect 30, 185–189. https://doi.org/10.1289/ehp.7930185.
[43] Ramírez, N., Cuadras, A., Rovira, E., Marcé Rosa, M., Borrull, F., 2011. Risk assessment related to atmospheric polycyclic aromatic hydrocarbons in gas and particle phases near industrial sites. Environ Health Perspect 119, 1110–1116. https://doi.org/10.1289/ehp.1002855.
[44] Rudich, Y., Donahue, N.M., Mentel, T.F., 2007. Aging of organic aerosol: bridging the gap between laboratory and field studies. Annu Rev Phys Chem 58, 321–352. https://doi.org/10.1146/annurev.physchem.58.032806.104432.
[45] Siudek, P., 2022. Seasonal distribution of PM2.5-bound polycyclic aromatic hydrocarbons as a critical indicator of air quality and health impact in a coastal-urban region of Poland. Sci Total Environ 827, 154375. https://doi.org/10.1016/j.scitotenv.2022.154375.
[46] Tham, Y.W.F., Takeda, K., Sakugawa, H., 2008. Polycyclic aromatic hydrocarbons (PAHs) associated with atmospheric particles in Higashi Hiroshima, Japan: influence of meteorological conditions and seasonal variations. Atmos Res 88, 224–233. https://doi.org/10.1016/j.atmosres.2007.10.015.
[47] Thornhill, D.A., de Foy, B., Herndon, S.C., Onasch, T.B., Wood, E.C., Zavala, M., et al., 2008. Spatial and temporal variability of particulate polycyclic aromatic hydrocarbons in Mexico City. Atmos Chem Phys 8, 3093–3105. https://doi.org/10.5194/acp-8-3093-2008.
[48] Turpin, B.J., Lim, H.-J., 2001. Species contributions to PM2.5 mass concentrations: revisiting common assumptions for estimating organic mass. Aerosol Sci Technol 35, 602–610. https://doi.org/10.1080/02786820119445.
[49] US EPA: Relative Potency Factors for Carcinogenic Polycyclic Aromatic Hydrocarbons (PAHs), Discussion and Recommendations for Consideration by the Cleanup Standards Scientific Advisory Board, PAH Workgroup, 2022. ⟨https://www.epa.gov/risk/relative-potency-factors-carcinogenic-polycyclic-aromatic-hydrocarbons-pahs⟩ (Last accessed, 20 December, 2024).
[50] US EPA: Assigning Values to Non-detected/Non-quantified Pesticide Residues in Human Health Food Exposure Assessments. Washington, DC, U.S. EPA, Office of Pesticide Programs, 2000. ⟨https://archive.epa.gov/pesticides/trac/web/pdf/trac3b012.pdf⟩ (Last accessed, 11 March, 2025).
[51] Vione, D., Barra, S., de Gennaro, G., de Rienzo, M., Gilardoni, S., Perrone, M.G., et al., 2004. Polycyclic aromatic hydrocarbons in the atmosphere: monitoring, sources, sinks and fate. II: Sinks and fate. Ann Chim 94, 257–268. https://doi.org/10.1002/adic.200490031.
[52] Wang, G., Wang, Y., Yin, W., Xu, T., Hu, C., Cheng, J., et al., 2020. Seasonal exposure to PM2.5-bound polycyclic aromatic hydrocarbons and estimated lifetime risk of cancer: a pilot study. Sci Total Environ 702, 135056. https://doi.org/10.1016/j.scitotenv.2019.135056.
[53] Wang, J. China Air Quality Online Monitoring and Analysis Platform. 2013. ⟨http://www.aqistudy.cn⟩. (Last accessed, 10 September 2024).
[54] Wang, J., Cao, J., Dong, Z., Guinot, B., Gao, M., Huang, R., et al., 2017. Seasonal variation, spatial distribution and source apportionment for polycyclic aromatic hydrocarbons (PAHs) at nineteen communities in Xi'an, China: the effects of suburban scattered emissions in winter. Environ Pollut 231, 1330–1343. https://doi.org/10.1016/j.envpol.2017.08.106.
[55] Wang, T., Li, B., Liao, H., Li, Y., 2021. Spatiotemporal distribution of atmospheric polycyclic aromatic hydrocarbon emissions during 2013–2017 in mainland China. Sci Total Environ 789, 148003. https://doi.org/10.1016/j.scitotenv.2021.148003.
[56] Wang, Y., Li, Q., Wang, S., Wang, Y., Luo, C., Li, J., et al., 2015. Seasonal and diurnal variations of atmospheric PAHs and OCPs in a suburban paddy field, South China: impacts of meteorological parameters and sources. Atmos Environ 112, 208–215. https://doi.org/10.1016/j.atmosenv.2015.04.047.
[57] Wang, Z., Fingas, M., Shu, Y.Y., Sigouin, L., Landriault, M., Lambert, P., et al., 1999. Quantitative characterization of PAHs in burn residue and soot samples and differentiation of pyrogenic PAHs from petrogenic PAHs—The 1994 mobile burn study. Environ Sci Technol 33, 3100–3109. https://doi.org/10.1021/es990031y.
[58] Warshawsky, D., 1999. Polycyclic aromatic hydrocarbons in carcinogenesis. Environ Health Perspect 107, 317–319. https://doi.org/10.1289/ehp.99107317.
[59] WHO: World Health Organization. Air Quality Guidelines for Europe. WHO Regional Office for Europe, 2000.
[60] WHO: World Health Organization. WHO Guidelines for Indoor Air Quality: Selected Pollutants. WHO Regional office for Europe, 2010.

[61] Williams, B.J., Goldstein, A.H., Kreisberg, N.M., Hering, S.V., 2010. In situ measurements of gas/particle-phase transitions for atmospheric semivolatile organic compounds. Proc Natl Acad Sci USA 107, 6676–6681. https://doi.org/10.1073/pnas.0911858107.

[62] Xie, M., Barsanti, K.C., Hannigan, M.P., Dutton, S.J., Vedal, S., 2013. Positive matrix factorization of PM2.5 - eliminating the effects of gas/particle partitioning of semivolatile organic compounds. Atmos Chem Phys 13, 7381–7393. https://doi.org/10.5194/acp-13-7381-2013.

[63] Xie, M., Hannigan, M.P., Barsanti, K.C., 2014. Gas/particle partitioning of n-alkanes, PAHs and oxygenated PAHs in urban Denver. Atmos Environ 95, 355–362. https://doi.org/10.1016/j.atmosenv.2014.06.056.

[64] Yamasaki, H., Kuwata, K., Miyamoto, H., 1982. Effects of ambient temperature on aspects of airborne polycyclic aromatic hydrocarbons. Environ Sci Technol 16, 189–194. https://doi.org/10.1021/es00098a003.

[65] Yan, D., Wu, S., Zhou, S., Tong, G., Li, F., Wang, Y., et al., 2019. Characteristics, sources and health risk assessment of airborne particulate PAHs in Chinese cities: a review. Environ Pollut 248, 804–814. https://doi.org/10.1016/j.envpol.2019.02.068.

[66] Yang, Y., Christakos, G., Yang, X., He, J., 2018. Spatiotemporal characterization and mapping of PM2.5 concentrations in southern Jiangsu Province, China. Environ Pollut 234, 794–803. https://doi.org/10.1016/j.envpol.2017.11.077.

[67] Yu, Y., He, S., Wu, X., Zhang, C., Yao, Y., Liao, H., et al., 2019. PM2.5 elements at an urban site in Yangtze River Delta, China: high time-resolved measurement and the application in source apportionment. Environ Pollut 253, 1089–1099. https://doi.org/10.1016/j.envpol.2019.07.096.

[68] Yu, Y., Ding, F., Mu, Y., Xie, M., Wang, Q. g, 2020. High time-resolved PM2.5 composition and sources at an urban site in Yangtze River Delta, China after the implementation of the APPCAP. Chemosphere 261, 127746. https://doi.org/10.1016/j.chemosphere.2020.127746.

[69] Zhang, J., He, X., Ding, X., Yu, J.Z., Ying, Q., 2022. Modeling secondary organic aerosol tracers and tracer-to-SOA ratios for monoterpenes and sesquiterpenes using a chemical transport model. Environ Sci Technol 56, 804–813. https://doi.org/10.1021/acs.est.1c06373.

[70] Zhang, Q., Zheng, Y., Tong, D., Shao, M., Wang, S., Zhang, Y., et al., 2019. Drivers of improved PM2.5 air quality in China from 2013 to 2017. Proc Natl Acad Sci USA 116, 24463–24469. https://doi.org/10.1073/pnas.1907956116.

[71] Zhang, Y., Tao, S., Shen, H., Ma, J., 2009. Inhalation exposure to ambient polycyclic aromatic hydrocarbons and lung cancer risk of Chinese population. Proc Natl Acad Sci USA 106, 21063–21067. https://doi.org/10.1073/pnas.0905756106.

[72] Zhou, Z., Wang, Z., Feng, W., Qin, C., Liao, H., Wang, Y., et al., 2024. Simulation of gas-particle partitioning of semi-volatile n-alkanes and PAHs in Nanjing, China, and Denver, United States: effects of vapor pressure and surface adsorption estimation. e2024JD041368 J Geophys Res Atmos 129. https://doi.org/10.1029/2024JD041368.

[73] Zhu, D., Hyun, S., Pignatello, J.J., Lee, L.S., 2004. Evidence for π−π electron donor−acceptor interactions between π-donor aromatic compounds and π-acceptor sites in soil organic matter through pH effects on sorption. Environ Sci Technol 38, 4361–4368. https://doi.org/10.1021/es035379e.